A New Globally Reconstructed Sea Surface Temperature Analysis Dataset since 1900

Lifan CHEN, Lijuan CAO, Zijiang ZHOU*, Dongbin ZHANG, and Jie LIAO

National Meteorological Information Center, China Meteorological Administration, Beijing 100081

(Received May 31, 2021; in final form October 8, 2021)

ABSTRACT

A new globally reconstructed sea surface temperature (SST) analysis dataset developed by the China Meteorological Administration (CMA-SST), available on 2° × 2° and monthly resolutions since 1900, is described and assessed in this study. The dataset has been constructed from a newly developed integrated dataset with denser and wider sampling of in situ SST observations and follows similar analysis techniques to the Extended Reconstructed SST, version 5 (ERSST.v5). Assessments show that the larger observation quantity of the input data source is beneficial to making the reconstructed SSTs more realistic than those reconstructed with ICOADS3.0 + GTS (International Comprehensive Ocean–Atmosphere Dataset 3.0 and Global Telecommunication System), especially in China's offshore sea area. Besides, a specific parameter for bias correction has been upgraded to be self-adaptive to the input data source, and serves as a mediator to improve the accuracy of the reconstructed SSTs. Generally, the reconstructed CMA-SST dataset is comparable to currently congeneric products. Its biases are similar to those of ERSST.v5, the Centennial Observation-Based Estimates of SST version 2 (COBE-SST2), the Hadley Centre Sea Ice and SST dataset version 2 (HadISST2), and the Hadley Centre SST dataset version 3 (HadSST3); and more specifically, they are closest to ERSST.v5 and lower than HadISST2 and HadSST3 at high latitudes of the Southern Hemisphere where in situ observations are limited. Moreover, its temporal characteristics, such as the year-to-year variations of globally averaged SST anomalies and time series of the Niño-3.4, Atlantic multidecadal oscillation, and Pacific decadal oscillation indices are also a good match to those of congeneric products. Although the warming rates of CMA-SST are a little higher in many regions over the periods 1900–2019 and 1950–2019, they are found to be acceptable and within the quantified uncertainties of ERSST.v5. However, there are noticeable differences in the strength and stability of spatial standard deviations among the various datasets, as well as low correlations between CMA-SST and the other products around 60°S where in situ sampling is very limited. These aspects necessitate further investigation and improvement of CMA-SST.

Key words: sea surface temperature, CMA-SST dataset, bias correction, reconstruction, climate change

Citation: Chen, L. F., L. J. Cao, Z. J. Zhou, et al., 2021: A new globally reconstructed sea surface temperature analysis dataset since 1900. *J. Meteor. Res.*, **35**(6), 911–925, doi: 10.1007/s13351-021-1098-7.

1. Introduction

Sea surface temperature (SST) is an essential climatic variable and plays an important role in climate change monitoring and assessment (Huang et al., 2016a). The 100-yr record of SST data, combined with air temperature data over land areas, is used to quantify and investigate global surface temperature change (IPCC, 2013). In addition, SST data are also used to monitor oceanic modes such as El Niño–Southern Oscillation (ENSO), the Pacific decadal oscillation (PDO), the Atlantic multidecadal oscillation (AMO), and the Indian Ocean dipole (Liu and Duan, 2017; Murphy et al., 2017; Ren et al., 2017; Huang and Wang, 2020). Moreover, the long record of SST data is also applied to verify climate models, and to force atmospheric general circulation models and assimilation systems (Lau and Nath, 2004; Zhou et al., 2009; Cai and Cowan, 2013).

Owing to the importance of SST in climate monitoring and modeling, a range of global gridded SST analysis

Supported by the National Key Research and Development Program of China (2017YFC1501801), National Innovation Project for Meteorological Science and Technology (CMAGGTD003-5), National Natural Science Foundation of China (41805128), and National Key Research and Development Program of China (2016YFA0600301).

*Corresponding author: zzj@cma.gov.cn

datasets have been developed in the past several decades by different groups, including the Extended Reconstructed SST (ERSST) by NOAA, the Centennial Observation-Based Estimates of SST (COBE-SST) by the Japan Meteorological Agency, the Hadley Centre SST dataset (HadSST), and the Hadley Centre Sea Ice and SST dataset (HadISST) (Ishii et al., 2005; Titchner and Rayner, 2014; Huang et al., 2017; Kennedy et al., 2019). These centennial-scale SST products adopt the increasing quantities of in situ SST observations as their primary data source. Besides, as the historical records of SST are a disparate collection of measurements taken by diverse means from different measurement platforms, all SST analysis datasets are systematically bias-adjusted to account for changes in measurement methods (Kennedy, 2014; Kent et al., 2017), and most products are analyzed by interpolation or a reconstruction procedure in order to fill data gaps and provide a construction of a globally complete estimate.

Although in compliance with similar analysis procedures, small but appreciable differences among the prominent SST analysis datasets are captured (Yasunaka and Hanawa, 2011). For example, the sea surface temperature anomalies (SSTAs) of ERSST.v4 were compared with those of HadSST3 and COBE-SST2, revealing estimates in ERSST.v4 that are about 0.1–0.2°C lower between 30°S and 30°N from approximately 1910 to 1970, 0.1°C higher to the south of 30°S before about 1920, and north of 30°N before around 1935 (Huang et al., 2015). Likewise, COBE-SST and ERSST.v3b exhibit an increasing trend from 1940 to 1980, while HadSST3 and COBE-SST2 decrease over this period (Hirahara et al., 2014). The differences may result from the input data sources, the quality control (QC) and bias adjustment methods applied, as well as the gridding and construction methodologies employed. Among them, the observation amounts and bias adjustment are asserted to have noticeable impacts on the uncertainty of the SST analyses. It is evident that different strategies of bias correction may call into question the existence of the recent global warming "hiatus" (Karl et al., 2015), and severe data sparseness is expected to cause large divergence in SST analysis, particularly in areas of low SST variability such as the western tropical Pacific, and in eddy-active regions (Hirahara et al., 2014).

Due to the practical significance of the differences and the knowledge of the close dependence of the SST products' quality on the spatiotemporal distribution of the observations and the applied analysis techniques (Hirahara et al., 2014), considerable ongoing efforts are made to upgrade these products. For example, eight progressive experiments, including new releases of data sources and a number of choices in aspects of QC, bias adjustment, and interpolation, have been substantively conducted toward ERSST.v5 from ERSST.v4 in order to seek improved estimates of the true SST state through time globally, regionally, and locally (Huang et al., 2017). Recently, the method used to estimate systematic errors and their uncertainties in HadSST3 has been revisited, since the differences between analyses remain larger than can be explained by the estimated uncertainties (Kennedy et al., 2019). The wider range of gridded SST estimations and datasets taking different strategies has been pointed out as being able to improve our understanding of structural uncertainty (Kent et al., 2017).

In this study, the development of a new globally reconstructed SST analysis dataset (referred to as the China Meteorological Administration global SST, or CMA-SST) is described and applied in constructing a new SST time series from the year 1900. The CMA-SST dataset follows a similar philosophy to ERSST.v5, in that the ship SSTs are first corrected by using nighttime marine air temperature (NMAT) as a comparator and then revised by more accurate buoy SSTs, and afterwards the merged ship and buoy SSTs are decomposed into low- and high-frequency components and reconstructed successively by different techniques to generate a homogenized and "globally complete" SST dataset at a 2° × 2° and monthly spatiotemporal resolution. The most substantial advance of CMA-SST is the utilization of a newly developed integrated dataset, which has clearly increased the level of in situ observational sampling of SST, especially in China's offshore and adjacent sea areas. Furthermore, a specific parameter for bias adjustment has been upgraded to be self-adaptive to the dataset and retain efficient input data for reconstruction.

The remainder of this paper describes the development and assessment of CMA-SST. The data sources used for the production and validation of CMA-SST are described in Section 2; the bias correction and reconstruction schemes are described in Sections 3 and 4, respectively; and the quality and characteristics of the SST analysis dataset are assessed and presented in Section 5. Finally, conclusions and some further discussion are provided in Section 6.

2. Data

Various datasets were used to develop and assess the CMA-SST dataset, consisting of the input dataset providing in situ SST observations, marine air temperature dataset applied to perform bias correction, spatially com-

plete SST dataset used to construct the SST climatology and derive empirical orthogonal teleconnection (EOT) patterns for reconstruction, sea-ice concentration data for refining reconstructed areas covered with ice, and independent SST analysis datasets for evaluation. The necessary details for each dataset are outlined in this section.

2.1 *Input dataset providing in situ SST observations*

Current datasets of historical SST analysis are largely based on in situ buoy and ship SST observations from the International Comprehensive Ocean–Atmosphere Dataset (ICOADS; Freeman et al., 2017) and the operational Global Telecommunication System (GTS). However, in CMA-SST, a new integrated Global Sea Surface Observation Dataset (GSSODS) developed by the National Meteorological Information Center is applied. In GSSODS, the integration of ICOADS3.0 and GTS receipts (ICOADS3.0 + GTS) has been upgraded by three supplementary data sources, including the ocean observations assimilated in the NCEP Climate Forecast System Reanalysis from 1979 to 2014 and the Global Data Assimilation System from 2015, and more importantly, the observational data located in China's offshore and adjacent sea areas from 1979 collected and released by the Centre for Marine-Meteorological and Oceanographic Climate Data/China, and China's commercial ship and offshore buoy observational data from 1999 collected by the China Meteorological Administration (CMA).

In ERSST.v5, the in situ observations derived from ICOADS3.0 and GTS are screened by checking the differences between the observations and the first guess, and the SST outliers with deviation larger than 4.5 times the standard deviation (STD) are removed (Huang et al., 2017). In GSSODS, however, each data source is first preprocessed with a comprehensive QC procedure consisting of extreme value checks, internal consistency checks, temporal consistency checks, spatial consistency checks, and eigenvalue checks, and then the different data sources are integrated to generate a long-term dataset with synthetic QC evaluation. After that, a further check similar to that applied in ERSST.v5 is adopted to screen out the remaining suspicious data wrongly flagged as correct. The two-step QC strategy is attached to GSSODS to ensure both the quantity and quality of in situ observations for further SST analysis.

To evaluate the sampling increment stemming from the three supplementary data sources in GSSODS, the monthly number and areal coverage of ship and buoy SST observations from 1979 are intercompared between GSSODS and ICOADS3.0 + GTS (Fig. 1). The integrated ICOADS3.0 + GTS dataset is treated with the same QC scheme applied in GSSODS, and only the data

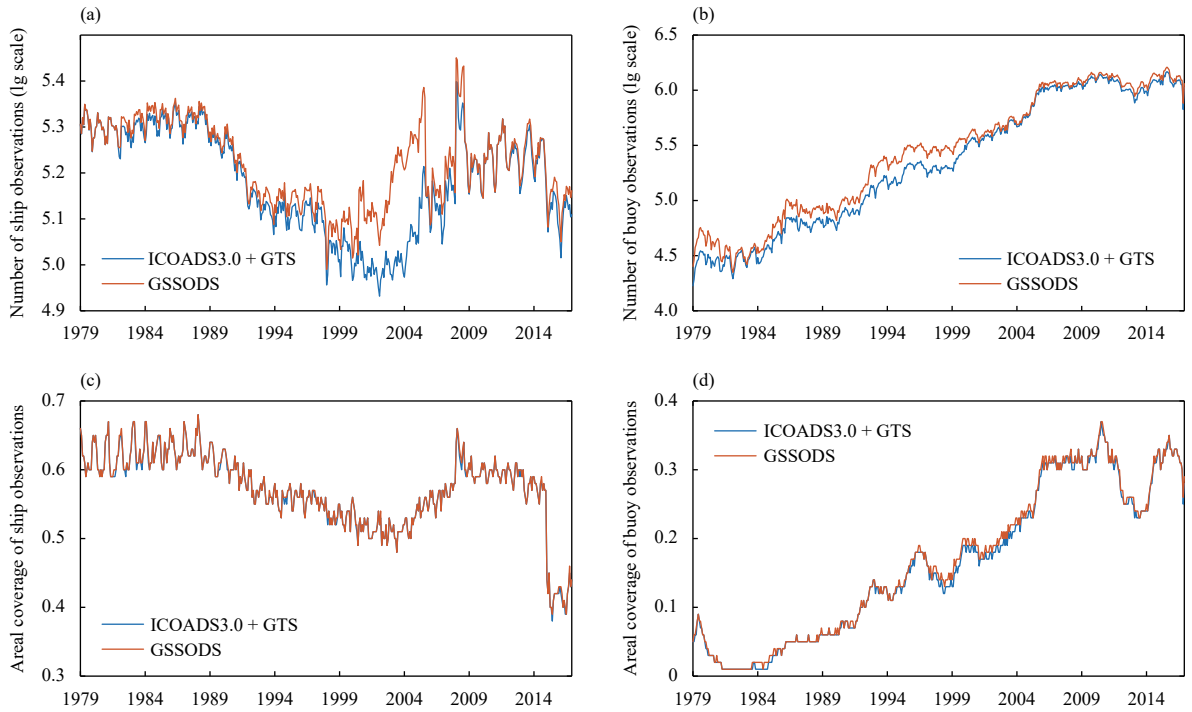

Fig. 1. Number (lg scale) and areal coverage of monthly (a, c) ship and (b, d) buoy SST observations in GSSODS and ICOADS3.0 + GTS from 1979. The areal coverage of monthly ship observations is the ratio of the area of 2° × 2° boxes containing ship SST observations to the total ocean area, as is the areal coverage of monthly buoy observations. Only correct data screened by the two-step QC procedure are shown.

flagged as correct by the two-step QC procedure are shown here. It can be seen that GSSODS includes more ship and buoy SST observations, especially in the 1990s–2000s and 1980s–1990s, respectively. Besides, the spatial coverage of ship SST observations is almost the same between GSSODS and ICOADS3.0 + GTS, while the spatial coverage of buoy SST observations is slightly higher in GSSODS, especially from the late 1990s. This indicates that the three supplementary data sources in GSSODS serve to provide denser ship SST observations and a slightly wider distribution of buoy observations. Also, in general, 17.1% of the global buoy SST observation increments are in China's offshore area, and the percentage is 11.7% for ship SST observation increments.

2.2 *Nighttime marine air temperature dataset*

The Hadley Centre and National Oceanography Centre NMAT dataset, version 2 (HadNMAT2) (https://www.metoffice.gov.uk/hadobs/hadnmat2/), is used as a comparator to perform ship SST bias adjustments. The dataset is a monthly global field of NMAT on a 5° × 5° grid. It is produced by using in situ measurements of marine air temperature made on board ships between 1 h after sunset and 1 h after sunrise, and bias corrections are applied to reduce the effects of spurious trends caused by changes in deck height on non-standard thermometer exposure (Kent et al., 2013). The NMAT is used to eliminate daytime biases due to heating of the ship deck (Smith and Reynolds, 2002).

2.3 *Spatially complete SST dataset*

The monthly NOAA Optimum Interpolation Sea Surface Temperature dataset, version 2 (OISST.v2), with a 1° × 1° spatial resolution (https://psl.noaa.gov/data/gridded/data.noaa.oisst.v2.html) from 1982 to 2011, is applied to create an intermediate climatology for a 30-yr SST climatology construction; and more importantly, the data are averaged by area-weighting to a 2° × 2° grid of CMA-SST and used to derive the EOT patterns for reconstruction of SST high-frequency components. The OISST.v2 dataset uses in situ and satellite SSTs plus SSTs simulated by sea-ice cover, and the satellite SSTs are adjusted based on the in situ data to compensate for sensor biases (Reynolds et al., 2007). The monthly fields are derived by linear interpolation of the weekly optimum interpolated OISST.v2 fields to daily fields, and then averaging the daily values over a month.

2.4 *Sea-ice concentration data*

The sea-ice concentration data are used to calibrate reconstructed SSTs over ice-covered areas in order to ensure that SST fields are not lower than the freezing point of sea water, especially over the polar regions, and are represented continuously between regions with and without sea ice (Hirahara et al., 2014; Huang et al., 2015). Monthly sea-ice concentrations from HadISST2 at a 1° × 1° spatial resolution for the period 1900–2015 (https://www.metoffice.gov.uk/hadobs/hadisst2/), and from OISST.v2 at a 1° × 1° resolution from 2016 (https://psl.noaa.gov/data/gridded/data.noaa.oisst.v2.html), are utilized in CMA-SST. As different development schemes are applied, there is discontinuity between HadISST2 and OISST.v2. Therefore, the shorter-term OISST sea-ice concentration is adjusted towards the HadISST2 sea-ice concentration by using the monthly varying averaged offsets between the two products from 2006 (Huang et al., 2017), and then both of them are averaged by area-weighting to the 2° × 2° grid of CMA-SST.

2.5 *Independent datasets used to compare with CMA-SST*

Intercomparisons of CMA-SST are made with several centennial-scale SST analysis datasets, including the monthly ERSST.v5 dataset (https://www.ncdc.noaa.gov/data-access/marineocean-data/extended-reconstructed-sea-surface-temperature-ersst-v5) with a 2° × 2° resolution, the monthly COBE-SST2 dataset (https://psl.noaa.gov/data/gridded/data.cobe2.html) with a 1° × 1° resolution, the monthly HadISST2 dataset (https://www.metoffice.gov.uk/hadobs/hadisst2/) with a 1° × 1° resolution, and the monthly HadSST3 dataset (https://www.metoffice.gov.uk/hadobs/hadsst3/) with a 5° × 5° resolution, from 1900 to 2019. All of the datasets are bias-adjusted to a homogenized long-term time series of global SST, and interpolation procedures are followed to generate globally complete fields of SST, except for HadSST3. The satellite-period SST reanalysis data of the European Space Agency Climate Change Initiative (CCI), level 4, version 1.1, from 1992 to 2010 (http://data.ceda.ac.uk/neodc/esacci/sst/data/lt/Analysis/L4/v01.1), are also used to evaluate CMA-SST. The CCI provides the mean SSTs at 20-cm depth on a daily 0.05° × 0.05° grid, and its SSTs are derived from the Along-Track Scanning Radiometer and the Advanced Very High Resolution Radiometer, which are largely independent from in situ observations (Merchant et al., 2014). The daily SSTs of CCI are first averaged to the monthly scale, and then by area-weighting to the 2° × 2° grid of CMA-SST.

3. Bias correction

Referring to the suite of ERSST datasets (Huang et al.,

2015, 2017), a large-scale statistical technique using comparisons with NMAT is applied to adjust the systematic biases of ship SSTs. The method was developed by Smith and Reynolds (2002, hereafter SR02) and based on an assumption that the large-scale differences between SST and NMAT are near constant over time, and the NMAT data are more straightforward to adjust and more homogeneous than the SST data to which it is being compared. In CMA-SST, the SR02 method is utilized because it can be formulated to further adjust the NMAT-based biases of ship SSTs by applying more accurate and homogenous buoy SSTs (Huang et al., 2017). The implementation of SR02 method generally contains five steps: (1) analysis of monthly differences between SST and NMAT, (2) outlier removal of SST–NMAT differences, (3) creation of a 30-yr climatology of the differences, (4) calculation of annual bias correction coefficients, and (5) estimation of monthly bias adjustments.

In CMA-SST, the in situ ship and buoy SSTs passing the two-step QC are respectively bin-averaged into monthly "superobservations" on a 2° × 2° grid to spread across the equator and meridian, and then ship SSTs before 2010 are corrected by the SR02 method and readjusted by a globally averaged offset between the NMAT-based and buoy-based bias estimates over the period 1990–2010, while ship SSTs after 2010 are directly adjusted by the annual globally averaged ship–buoy SST differences with a temporal filter (Huang et al., 2017). The bias adjustments by the SR02 method are conducted in the 5° × 5° grid boxes of HadNMAT2 and then linearly interpolated to the 2° × 2° grid of CMA-SST. While conducting the SR02 technique, the monthly climatology of the SST–NMAT differences is calculated as the temporal average from 1981 to 2010 and then spatially smoothed and missing locations filled by optimal interpolation (OI); the annual bias correction coefficients are fitted by minimizing the global error of the estimated SST–NMAT differences compared to the observed differences and temporally smoothed by the same scheme as used in ERSST.v5 (Huang et al., 2017); and the monthly adjustments are estimated as the annual coefficient multiplied by the climatology for each calendar month. The SR02 method is interrupted in 2010 because the HadNMAT2 dataset has only released its NMAT data up to 2010. After adjustments, ship SSTs are combined with buoy SSTs by weights based on the respective numbers of valid ship and buoy observations within each 2° × 2° grid box, and the number of buoy observations is multiplied by a factor of 6.8, which was determined by the ratio of random error variances of ship and buoy observations (Huang et al., 2015).

It is notable that a spatiotemporal unified threshold is applied to exclude the outliers of SST–NMAT differences in the original SR02 method (Smith and Reynolds, 2002), but a previous investigation showed that the threshold tends to screen out too many of the differences, especially in China's offshore sea area (Chen et al., 2019). Hence, a superior scheme reconciling the temporal 3σ rule with spatial neighbor-based QC means of gridded data (Rayner et al., 2003) is utilized to refine the thresholds applied in CMA-SST. The refined thresholds have three advantages: (1) they are self-adaptive for a comprehensive consideration of both the spatial and temporal flexibility for each grid box; (2) abnormal superobservations with enough valid adjacent grids are adjusted to preserve as many effective data as possible; and (3) they are self-adaptive to the input data source, especially for the compilation of supplementary observation data in China's offshore sea area in the GSSODS dataset. The monthly percentage of 2° × 2° SST–NMAT differences excluded by the unified threshold and refined thresholds are intercompared (Fig. 2), from which we can see that

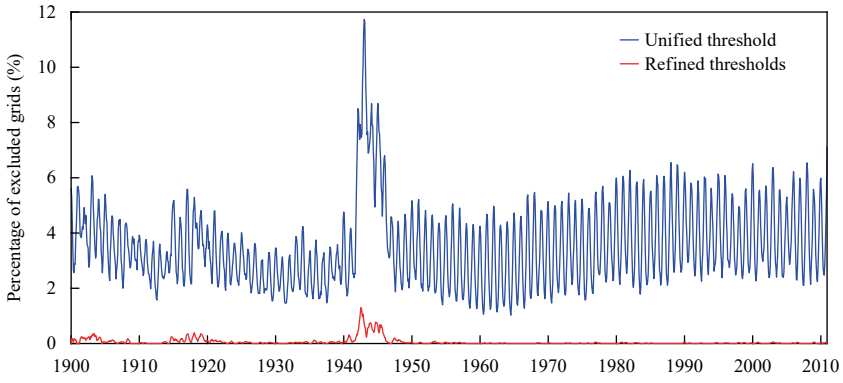

Fig. 2. Monthly percentage of 2° × 2° SST–NMAT differences excluded by the unified threshold and refined thresholds in the period 1900–2010.

the refined thresholds retain many of the SST–NMAT differences excluded by the unified threshold owing to their spatiotemporal flexibility and further retrieval of some outliers by weighting the valid neighboring grid boxes.

4. Reconstruction methods

4.1 *Construction of a 30-yr climatology*

A monthly climatology is produced for the 1981–2010 base period, utilizing the merged ship and buoy SST superobservations. The construction method is nearly identical to that used by Smith and Reynolds (1998), in which a 30-yr SST climatology is produced from two intermediate climatologies: an SST climatology developed from in situ data and an SST climatology derived from OISST that uses in situ and satellite data. The construction procedures are:

(1) A monthly climatology of in situ data is computed by averaging the filled months for the desired base period, 1981–2010. As the in situ climatology is confined to regions with sufficiently filled superobservations (at least two for each three-decade period in the desired base period: 1981–1990, 1991–2000, and 2001–2010), it is unable to be defined for every ocean grid box.

(2) An OI climatology is formed for each calendar month by averaging all the OISST.v2 data at 1° × 1° resolution (Section 2.3) for that month over the period 1982–2010 and resampling to the same 2° grid of the in situ climatology.

(3) The differences between the two climatologies are computed for each month and set as 0 if there is no in situ climatology.

(4) The differences are spatiotemporally smoothed and noise-reduced by moving-area averaging and a Fourier series fit.

(5) The OI climatology is adjusted to the in situ climatology by the smoothed differences, and then the missing in situ climatology is filled with the adjusted result.

(6) The filled in situ climatology is smoothed by binomial interpolation for the potential discontinuity between the in situ and OI climatologies.

4.2 *Reconstruction of SSTAs*

The merged SSTs are converted to SSTAs by subtracting the constructed 30-yr climatology at their grid location, and then the SSTAs are analyzed by methods specially designed to recover features from the inadequate global coverage of in situ sampling. The analyses are always conducted by decomposing the SSTAs into low- and high-frequency components and reconstructing them separately, because stationary statistics used for the high-frequency analysis are based on data in the satellite era only, which may not be adequate for spanning the inter-decadal variations of the low-frequency component (Rayner et al., 2003; Hirahara et al., 2014; Huang et al., 2017). The reconstruction procedures are essential to generate SST variations that are more realistic in areas devoid of observations and to facilitate studies of the regional structure and interannual variability of associated phenomena (e.g., ENSO and its effects) in terms of making them more objective and reliable, especially with respect to the sparse and irregular in situ data in the early period (Huang et al., 2016b, 2019).

In CMA-SST, the low-frequency component is reconstructed by a scheme that synthesizes the different procedures applied in the various ERSST versions (Smith and Reynolds, 2003; Huang et al., 2015, 2017). Its practical operational procedures are to: (1) calculate the running mean of the monthly SSTAs within a 26° × 26° spatial window with at least five filled superobservations; (2) define the annual mean SSTA fields when there are no less than two monthly superobservations; (3) screen the annual SSTAs and fill the missing superobservations by averaging the neighbors within 10° of longitude, 6° of latitude, and 3 yr in time; (4) filter the annual SSTAs via a three-point binomial filter in both the longitudinal and latitudinal direction, and then with a 15-yr median filter; and (5) set the missing superobservations as 0 and filter the SSTAs via a three-point binomial filter in both the longitudinal and latitudinal directions again.

The high-frequency component is retrieved from the SSTAs by subtracting the low-frequency component, and is then reconstructed by using a similar scheme as that applied in ERSST.v5 (Huang et al., 2017). The reconstruction procedures are to: (1) derive the 140 leading EOT modes (van den Dool et al., 2000), which are localized empirical orthogonal functions (EOFs) derived from the detrended monthly OISST data (Section 2.3) and restricted in the domain to a spatial scale of 3000 km in latitude and 6000–8000 km in longitude; (2) filter the missing SSTAs of the high-frequency component by averaging the valid pre- and post-current-month data; (3) linearly fit the filtered SSTAs to the trained EOTs in a least-squares sense, in which the EOT modes are first screened and accepted if the observations support more than 0.1 of their variance ratios; and (4) filter the missing fitting coefficients by averaging the valid pre- and post-current-month coefficients weighted by a lag-1 autocorrelation coefficient. The EOT technique is chosen over the EOF because it has higher degree of freedom and the order of the EOTs is free. More specifically, EOT yields solu-

tions of multiple linear regression that are orthogonal in one direction (either in space or time), and certain modes (base points) can be picked first (van den Dool et al., 2000).

Finally, the reconstructed low- and high-frequency SSTAs from 1900 are combined, and the sea-ice concentration data are incorporated to relax the reconstructed SSTs in partially ice-covered areas towards the freezing point. The reconstructed SSTs of the grid boxes with a sea-ice concentration greater than 0.9 are set to the freezing point of −1.8°C (grid boxes in the Great Lakes area are set to 0°C); the reconstructed SSTs with a sea-ice concentration between 0.6 and 0.9 are adjusted by using a piecewise linear method; and the reconstructed SSTs with a sea-ice concentration of less than 0.6 stay the same (Huang et al., 2017).

5. Results

5.1 *Influences of increasing observations and refined thresholds*

The advantages of the increased sampling in the GSSODS dataset and the efficient recovery of observations by the refined thresholds used for bias correction are clearly displayed in Figs. 1, 2; however, their influence on the accuracy of the reconstructed SSTs needs to be more definitively assessed. To quantitatively evaluate the impacts, SSTs are reconstructed with the input dataset of GSSODS but by the unified threshold and refined thresholds separately, and by the refined thresholds but with the input dataset being ICOADS3.0 + GTS or GSSODS. Thereafter, the biases relative to observed buoy SSTs are estimated, and the globally averaged biases from 1999 (the coverage of buoy superobservations becomes sufficient for comparison by no less than 15% from 1999) for each of the two sets of monthly reconstructed SSTs are intercompared (Fig. 3). It can be seen that the biases of the SSTs reconstructed by the refined thresholds are slightly lower than those reconstructed by the unified threshold, and the differences are locally clear from about 2011 (Fig. 3a). Comparatively, the biases of the SSTs reconstructed with the input dataset of GSSODS are obviously lower than those reconstructed with ICOADS3.0 + GTS throughout the analysis period, and the average reduction in bias is about 0.02°C (Fig. 3b). This indicates that the refined thresholds serve as a mediator to retain some efficient observations and have a limited capacity to improve the fidelity of the reconstructed SSTs; whereas the increased in situ sampling in GSSODS has straightforward and more stable influences on the reconstructed SSTs, being able to improve the reconstruction accuracy noticeably. Generally speaking, producing CMA-SST with the input dataset of GSSODS and the refined thresholds for bias correction is sensible.

The monthly root-mean-square errors (RMSEs) relative to the observed buoy SSTs are estimated for the SSTs reconstructed by the refined thresholds but with the input dataset being ICOADS3.0 + GTS or GSSODS, and the spatial distribution of the average RMSE difference from 1999 is shown in Fig. 4a. It can be seen that the SSTs reconstructed by ICOADS3.0 + GTS have obviously higher RMSE than those by GSSODS in the northern areas of the Pacific and Atlantic, especially in China's offshore and adjacent sea areas. This spatial pattern is consistent with the simultaneous spatial distribution of the in situ SST sampling increments from ICOADS3.0 + GTS to GSSODS, including the total number of in situ ship SST observations in each 2° × 2° grid box (Fig. 4b)

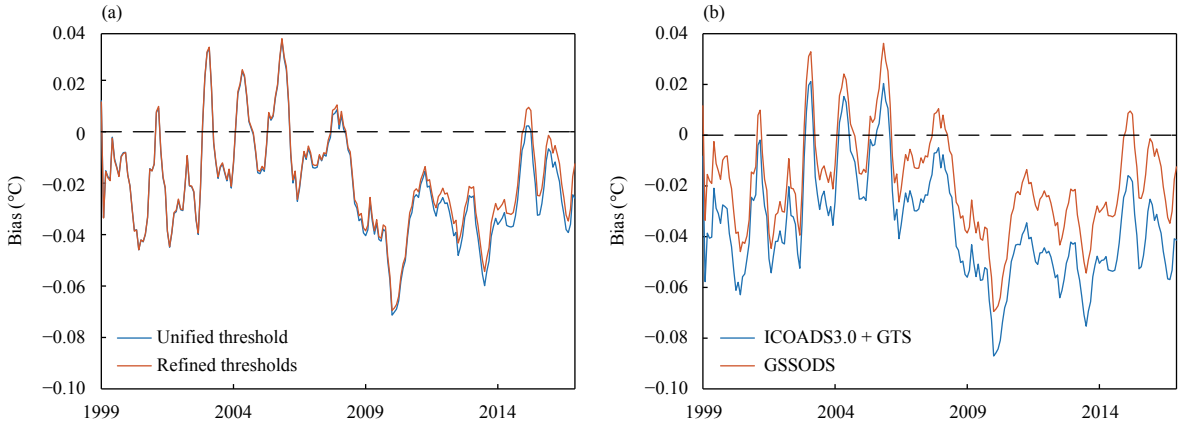

Fig. 3. Globally averaged biases of reconstructed SSTs from 1999. The biases are relative to buoy SSTs and intercompared between (a) SSTs reconstructed with the input dataset of GSSODS but by the unified threshold and refined thresholds, and (b) SSTs reconstructed by the refined thresholds but with the input datasets being ICOADS3.0 + GTS or GSSODS. A 5-month moving average filter is applied in the plots.

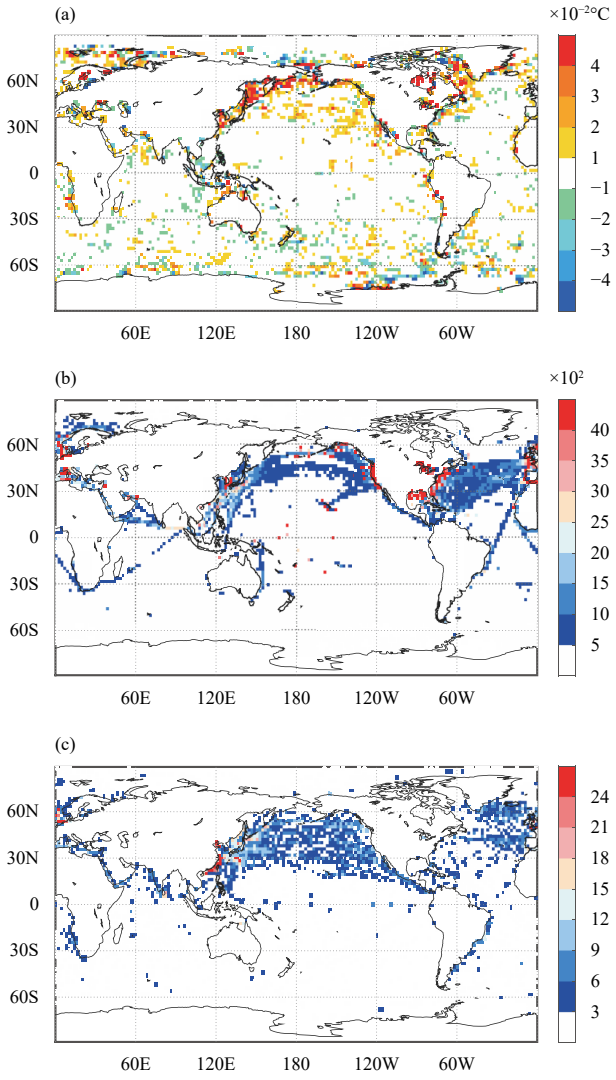

Fig. 4. (a) Averaged RMSE (°C) differences between SSTs reconstructed by ICOADS3.0 + GTS and GSSODS from 1999, and the simultaneous number differences between GSSODS and ICOADS3.0 + GTS for (b) in situ ship SST observations in each 2° × 2° grid box and (c) monthly 2° × 2° buoy grid boxes containing observations. The RMSE is relative to the buoy SSTs.

and the total number of monthly 2° × 2° buoy grids containing SST observations (Fig. 4c). This further indicates that the increased sampling in GSSODS is conducive to making the reconstructed SSTs more realistic than those reconstructed with ICOADS3.0 + GTS.

5.2 *Assessment of the reconstructed CMA-SST*

The monthly biases relative to observed buoy SSTs in the period 1999–2019 and CCI reanalysis data in the period 1992–2010 are estimated, and the globally averaged biases are compared among CMA-SST, ERSST.v5, COBE-SST2, HadISST2, and HadSST3 (Fig. 5). Generally, CMA-SST has biases roughly similar to the ERSST.v5, COBE-SST2, HadISST2, and HadSST3 products. All the datasets tend to be cooler than the in situ buoy observations and warmer than the independent CCI reanalysis data. Comparatively, the biases of CMA-SST are closest to those of ERSST.v5, due to the application of similar bias correction and reconstruction techniques. Both are closer to 0°C than the biases of the other products, particularly for the bias estimations relative to the independent CCI reanalysis data. In the main, CMA-SST shows relatively homogeneous biases of less than 0.08°C in relation to buoy SSTs, and positive biases of less than 0.16°C and with an apparent decrease through time in relation to the CCI data. Besides, HadSST3, with the smoothest spatial resolution (5° × 5°), shows substantially higher biases than the other products, particularly for the bias estimations relative to buoy SSTs, possibly because of its non-reconstruction of in situ observations with random noise, which needs further investigation.

The spatial distributions of the averaged biases relative to buoy SSTs over the period 1999–2019 and CCI reanalysis data over the period 1992–2010 are compared among the CMA-SST, ERSST.v5, COBE-SST2, HadISST2, and HadSST3 datasets (Fig. 6). Generally, CMA-SST produces a similar spatial pattern and strength of biases to the other products, especially the larger biases in western boundary current regions and at high latitudes, and its bias distributions are most similar to those of ERSST.v5. Comparatively, CMA-SST and ERSST.v5 are systematically cooler in the Arctic area relative to buoy SSTs, and most of the biases exceed 0.4°C; whereas COBE-SST2, HadISST2, and HadSST3 produce both negative and positive biases to the same degree of magnitude in this region. Besides, CMA-SST, ERSST.v5, and COBE-SST2 have clearly lower biases than HadISST2 and HadSST3 at high latitudes of the Southern Hemisphere. Furthermore, the biases of all datasets are mostly within −0.1 to 0.1°C at low and middle latitudes, except for HadSST3, which has clearly higher biases in the central-eastern equatorial Pacific Ocean. Meanwhile, in relation to CCI reanalysis data, CMA-SST and ERSST.v5 have their lowest biases within −0.1 to 0.1°C in the Arctic area, closely followed by HadISST2 and HadSST3 and then COBE-SST2 with obviously higher biases in this region. Besides, comparable biases among CMA-SST, ERSST.v5, and COBE-SST2 are apparent at high latitudes of the Southern Hemisphere, as well as in low and middle latitudes, while distinctly larger biases in these regions are captured in HadSST3 and slightly higher biases at high latitudes of the Southern Hemisphere are captured in HadISST2. Overall, the accuracy of CMA-SST is no less than other current congeneric

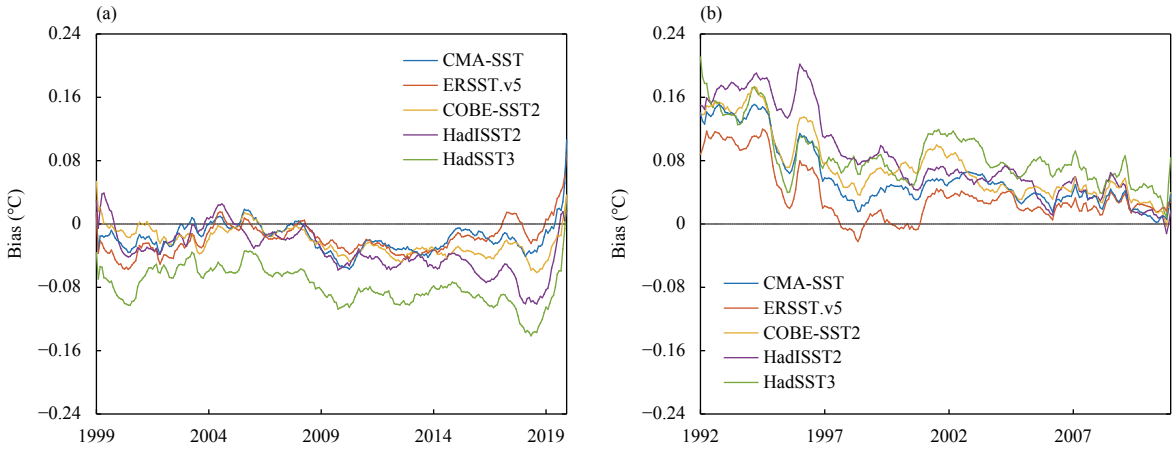

Fig. 5. Globally averaged biases of monthly CMA-SST, ERSST.v5, COBE-SST2, HadISST2, and HadSST3 data relative to (a) buoy SSTs in the period 1999–2019 and (b) CCI reanalysis data in the period 1992–2010. COBE-SST2, HadISST2, HadSST3, and CCI are resampled to the same 2° grid of CMA-SST, and a 12-month moving average filter is applied in the plots.

products.

The globally averaged SSTAs of monthly CMA-SST, ERSST.v5, COBE-SST2, HadISST2, and HadSST3 data and twice their standard deviation (2STD) in the period 1900–2019 are estimated and compared (Fig. 7). The SSTAs have been set to be relative to their own climatologies over 1981–2010. Generally, CMA-SST shares similar trends to the other products, with two significant warming trends before the mid-1940s and after the mid-1970s, and a shutdown of the warming trend between them is captured for all datasets. The year-to-year variations of CMA-SST are also similar to those of the other products. For the pre-1965 period, the globally averaged SSTAs of CMA-SST tend to be slightly lower than in the other datasets, but the differences are within the 95% confidence interval of the differences for all the datasets (shown in the lower panel), and these differences do not change the overall character of the SSTA variation through the analysis period. After the mid-1960s, most of the SSTAs of CMA-SST are identical to those of the other products, accompanied by a notable decrease in STD for all the datasets.

The trends of annually and area-weighted averaged SSTAs and their uncertainties at the 95% confidence level are estimated and compared among the CMA-SST, ERSST.v5, COBE-SST2, HadISST2, and HadSST3 datasets (Tables 1–3). The 95% confidence interval was calculated by using the IPCC's method of accounting for the uncertainty of a trend estimation (Karl et al., 2015). Significant warming rates are detected in all the datasets over the various regions of different latitudes for periods including 1900–2019, 1950–2019, and 2000–2019. In addition, an accelerating warming rate of globally averaged SSTAs is captured in all analyzed datasets by a higher warming rate in the more recent period. Furthermore, the accelerating warming rates are also detected in all latitudinal zones except the region of 60°–20°S in the CMA-SST dataset, which reflects the statistics derived from the other products including HadISST2 and HadSST3. Besides, CMA-SST exhibits an ocean warming rate within the rates of the other four products in all the different regions in the period 2000–2019, the region 60°–90°N in the period 1950–2019, and the regions 60°–90°N and 60°–20°S in the period 1900–2019. Apart from these regions, CMA-SST shows a slightly higher warming rate than the other products; however, the warming rates are within the quantified uncertainties of ERSST.v5.

The Niño-3.4 index over the period 1950–2019 is estimated and compared among the CMA-SST, ERSST.v5, COBE-SST2, HadISST2, and HadSST3 datasets (Fig. 8a). The Niño-3.4 index acts as one of several ENSO indicators and is based on the average SSTA in the region 5°S–5°N, 170°–120°W (Trenberth, 1997; Yasunaka and Hanawa, 2011). Overall, the SSTA time series of CMA-SST in the Niño-3.4 region shows no significant differences with those of the other products, including the peak times and values associated with ENSO events. In addition, the AMO index and the PDO index of CMA-SST over 1950–2019 are also compared with those of the other products (Figs. 8b, c). The AMO index is based on the average SSTA in the region 0°–70°N, 80°W–0° and has been identified as an indicator of multidecadal SST changes over the North Atlantic Ocean (Yasunaka and Hanawa, 2011). It can be seen that the SSTA time series of CMA-SST shows an identical trend in the AMO region to the other products. A decrease in SSTAs between the early 1960s and the mid-1970s and an increase with

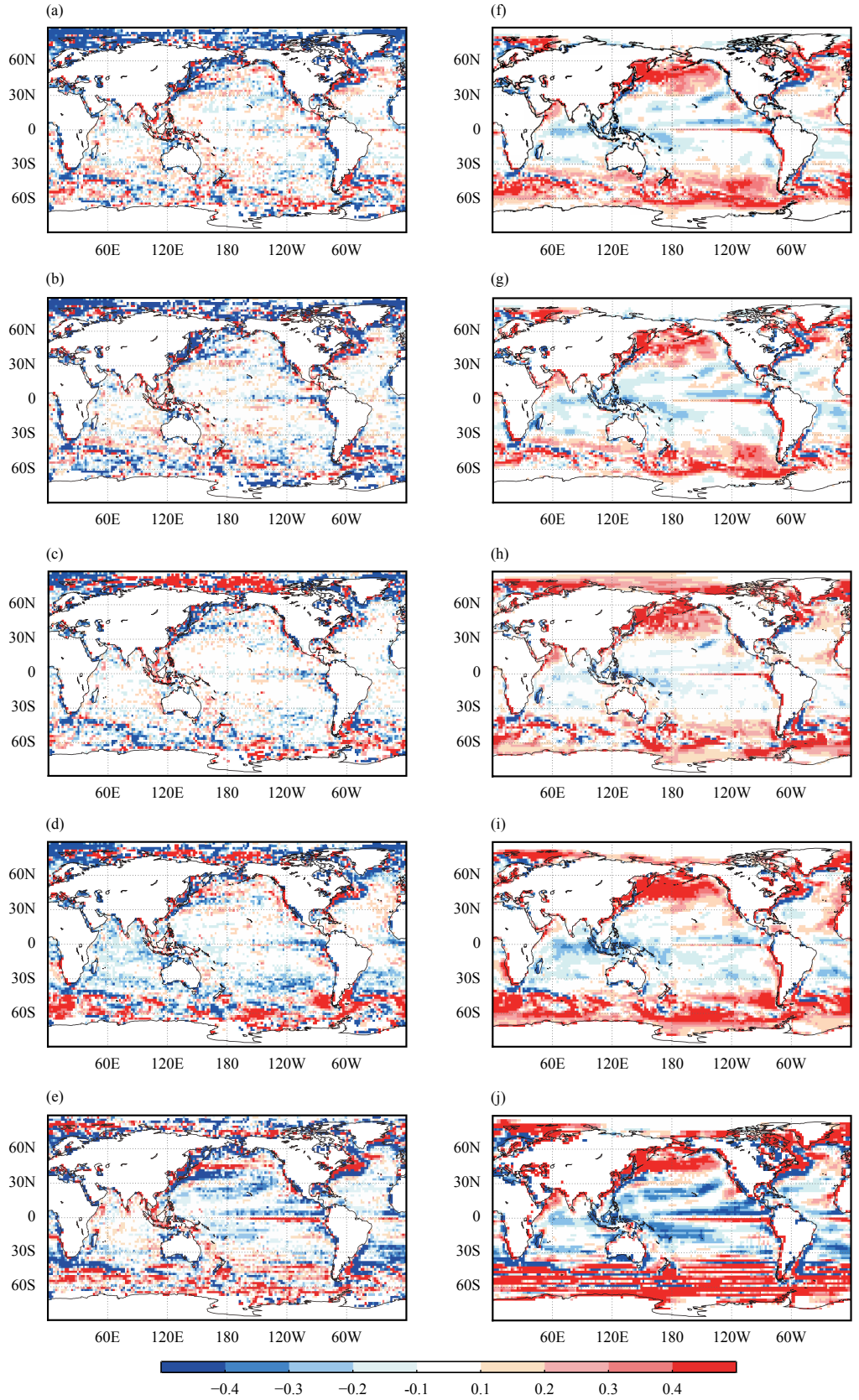

Fig. 6. Averaged biases (°C) of (a) CMA-SST, (b) ERSST.v5, (c) COBE-SST2, (d) HadISST2, and (e) HadSST3 relative to buoy SSTs over the period 1999–2019. (f–j) As in (a–e), but for the averaged biases relative to CCI reanalysis data over the period 1992–2010. COBE-SST2, HadISST2, HadSST3, and CCI are resampled to the same 2° grid of CMA-SST.

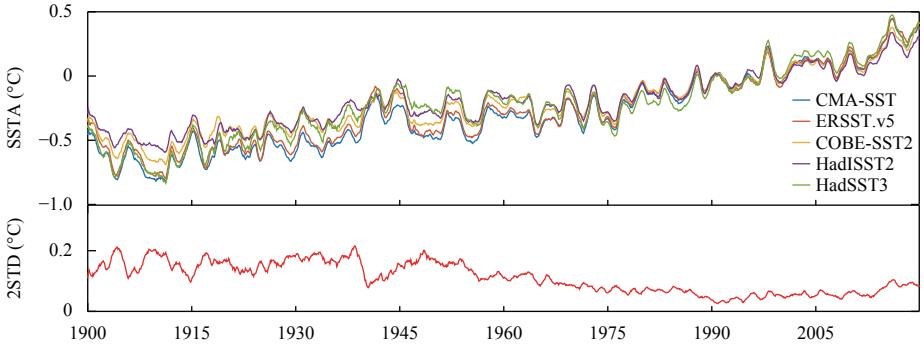

Fig. 7. Globally averaged SSTAs of monthly CMA-SST, ERSST.v5, COBE-SST2, HadISST2, and HadSST3 data (upper panel) and twice their standard deviation (2STD; lower panel) in the period 1900–2019. The SSTAs have been set to be relative to their own climatologies over 1981–2010, and a 12-month moving average filter is applied in the plots.

Table 1. Trends (°C century^{-1}) over 1900–2019 and their uncertainties at the 95% confidence level of annually and area-weighted averaged SSTAs. The SSTAs have been set to be relative to their own climatologies over 1981–2010, and values in bold indicate trends passing the 0.05 significance level based on the *F*-test

	CMA-SST	ERSST.v5	COBE-SST2	HadISST2	HadSST3
90°S–90°N	**0.79** ± 0.055	**0.74** ± 0.061	**0.61** ± 0.046	**0.55** ± 0.042	**0.71** ± 0.074
60°S–60°N	**0.84** ± 0.057	**0.78** ± 0.064	**0.63** ± 0.049	**0.58** ± 0.045	**0.73** ± 0.073
60°–90°N	**0.42** ± 0.139	**0.53** ± 0.164	**0.94** ± 0.177	**0.55** ± 0.091	**0.37** ± 0.158
20°–60°N	**0.80** ± 0.149	**0.71** ± 0.150	**0.68** ± 0.115	**0.64** ± 0.114	**0.73** ± 0.155
20°S–20°N	**0.83** ± 0.079	**0.79** ± 0.083	**0.61** ± 0.067	**0.50** ± 0.069	**0.64** ± 0.071
60°–20°S	**0.86** ± 0.089	**0.80** ± 0.089	**0.62** ± 0.055	**0.64** ± 0.046	**0.88** ± 0.070

Table 2. As in Table 1, but for trends and uncertainties (°C century^{-1}) over 1950–2019

	CMA-SST	ERSST.v5	COBE-SST2	HadISST2	HadSST3
90°S–90°N	**1.06** ± 0.058	**1.01** ± 0.063	**0.81** ± 0.058	**0.71** ± 0.058	**0.88** ± 0.113
60°S–60°N	**1.11** ± 0.062	**1.05** ± 0.067	**0.82** ± 0.062	**0.75** ± 0.062	**0.89** ± 0.110
60°–90°N	**0.93** ± 0.194	**1.09** ± 0.254	**1.63** ± 0.106	**0.92** ± 0.139	**0.78** ± 0.280
20°–60°N	**0.99** ± 0.277	**0.93** ± 0.287	**0.74** ± 0.225	**0.71** ± 0.257	**0.86** ± 0.314
20°S–20°N	**1.21** ± 0.096	**1.14** ± 0.098	**0.95** ± 0.090	**0.88** ± 0.094	**0.91** ± 0.109
60°–20°S	**1.06** ± 0.106	**1.01** ± 0.086	**0.72** ± 0.066	**0.63** ± 0.056	**0.93** ± 0.074

Table 3. As in Table 1, but for trends and uncertainties (°C century^{-1}) over 2000–2019

	CMA-SST	ERSST.v5	COBE-SST2	HadISST2	HadSST3
90°S–90°N	**1.54** ± 0.228	**1.72** ± 0.208	**1.39** ± 0.178	**1.12** ± 0.174	**1.38** ± 0.195
60°S–60°N	**2.13** ± 0.124	**2.93** ± 0.129	**1.61** ± 0.070	**2.16** ± 0.091	**2.18** ± 0.117
60°–90°N	**2.13** ± 0.124	**2.93** ± 0.129	**1.61** ± 0.070	**2.16** ± 0.091	**2.18** ± 0.117
20°–60°N	**2.47** ± 0.274	**2.57** ± 0.272	**1.88** ± 0.246	**1.58** ± 0.242	**1.95** ± 0.315
20°S–20°N	**1.80** ± 0.334	**1.91** ± 0.339	**1.57** ± 0.313	**1.53** ± 0.305	**1.30** ± 0.306
60°–20°S	**0.84** ± 0.204	**1.11** ± 0.127	**1.08** ± 0.179	**0.49** ± 0.069	**0.92** ± 0.123

fluctuations after the mid-1970s are captured in all datasets in the AMO region. Besides, a cool AMO phase in the 1960s–1980s and a warm phase from the late 1990s are also captured in all datasets. The PDO is often described as a long-lived El Niño-like pattern of Pacific climate variability, and the index is defined as the leading principal component (EOF) of North Pacific (20°–70°N, 110°E–100°W) monthly SSTA variability (Zhang et al., 1997). It shows that the monthly PDO index of CMA-SST is consistent with the other products, which proves the capability of CMA-SST to monitor the climate variation signal from interannual to decadal scales.

The correlation coefficients between the monthly SSTAs from CMA-SST and those from ERSST.v5, COBE-SST2, HadISST2, and HadSST3 for the period 1900–2019 are calculated and their spatial distributions are shown in Fig. 9. Generally, CMA-SST shows the best agreement with ERSST.v5, with high correlation coefficients (> 0.8) in most regions of the global ocean, especially at high latitudes of the Southern Hemisphere near sea ice with limited in situ sampling, and this is mainly due to the application of similar analysis techniques. Next is COBE-SST2, with which CMA-SST also has high correlation coefficients (> 0.8) in most of the low–mid-latitudes, especially the central and eastern tropical Pacific, the high-latitude North Pacific and North Indian

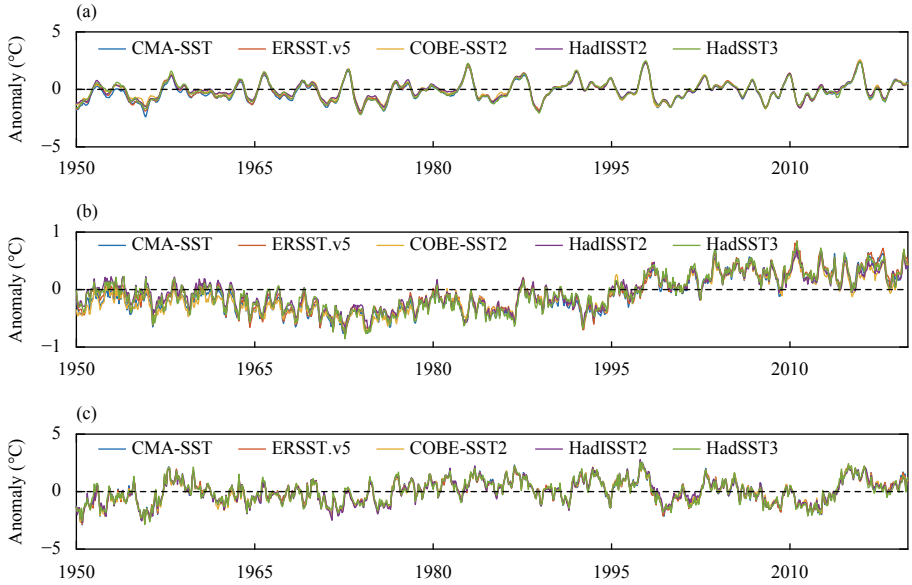

Fig. 8. Averaged SSTAs in the (a) Niño-3.4 and (b) AMO regions, and (c) the PDO index of CMA-SST, ERSST.v5, COBE-SST2, HadISST2, and HadSST3 in the period 1950–2019. The SSTAs are set to be relative to their own climatologies over 1981–2010, and a 5-month running mean filter is applied in (a).

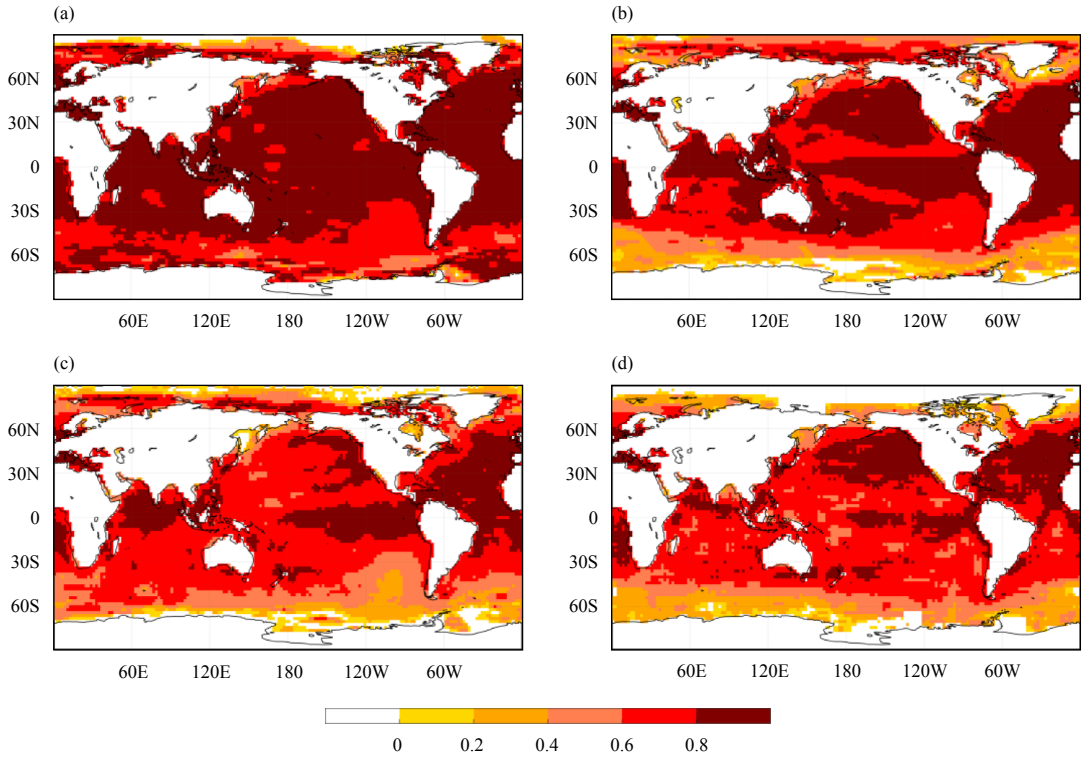

Fig. 9. Correlations between the monthly SSTAs from CMA-SST and those from (a) ERSST.v5, (b) COBE-SST2, (c) HadISST2, and (d) HadSST3 for the period 1900–2019. The SSTAs are set to be relative to their own climatologies over 1981–2010, and COBE-SST2, HadISST2, and HadSST3 are resampled to the same 2° grid of CMA-SST. The correlation coefficients shown are those passing the 0.05 significance test.

Ocean, the Atlantic, and the oceans around Australia. Overall, the central and eastern tropical Pacific and North Atlantic regions are detected with similar and relatively high correlation coefficients between CMA-SST and the other four products. Around 60°S, CMA-SST has low correlation coefficients (< 0.2) with COBE-SST2, HadISST2, and HadSST3, which is mainly due to the limited observational data in this area.

The spatial STDs of the monthly SSTAs from CMA-SST, ERSST.v5, COBE-SST2, HadISST2, and HadSST3 from 1900 to 2019 are calculated and presented in Fig. 10. Although the spatial resolution of HadSST3 is lowest (5° × 5°), its spatial heterogeneity is largest since it is the only dataset without reconstruction and is vulnerable to the random noise of in situ observations (Figs. 5, 6). On the contrary, the spatial heterogeneities of CMA-SST, ERSST.v5, COBE-SST2, and HadISST2 are close and significantly lower than that of HadSST3, because their random noise of in situ observations is smoothed by the reconstruction procedures to some extent. By comparison, HadISST2 shows obviously higher stability of spatial heterogeneity among the four close datasets; its spatial STDs are more stable between the pre- and post-1960s periods, while CMA-SST, ERSST.v5, and COBE-SST2 have higher spatial heterogeneity in the pre-1960s period, when the in situ sampling is relatively sparse. The differences in the strength and stability of the spatial STDs might be due to the reconstruction procedures accounting for the spatial patterns of global and regional SSTAs, which needs further investigation.

6. Conclusions and discussion

In this study, a newly developed globally reconstructed SST analysis dataset, CMA-SST, available from 1900, is described and assessed. It follows a similar philosophy to ERSST.v5, in that ship SSTs are first corrected by using NMAT as a comparator and then revised by more accurate buoy SSTs, and afterwards the merged ship and buoy SSTs are decomposed into low- and high-frequency components and reconstructed successively by different techniques. The bias correction and reconstruction procedures promote CMA-SST to be homogenized and "globally complete" at a 2° × 2° and monthly spatiotemporal resolution. The most substantial advance of CMA-SST is the utilization of GSSODS as the input dataset, which serves as an upgrade on the two commonly used data sources of ICOADS3.0 and GTS by merging them with three supplementary data sources, and moreover employs a synthesized QC strategy to guarantee the quality of in situ observations. Compared to the integration of ICOADS3.0 and GTS, GSSODS has denser ship SST observations and a wider distribution of buoy SST observations. The increased sampling is found to be conducive to making the reconstructed SSTs more realistic than the SSTs reconstructed with ICOADS3.0 + GTS, especially in China's offshore sea area. Besides, a parameter used to detect and exclude outliers of SST–NMAT differences for bias correction has been upgraded. Compared to the original unified threshold, the refined thresholds are self-adaptive to GSSODS and serve as a mediator to retain efficient observations and improve the fidelity of the reconstructed SSTs in a limited capacity.

Evaluations with respect to a range of aspects highlight the comparability of CMA-SST to current international congeneric products. First, the biases of CMA-SST are roughly the same as those of the ERSST.v5, COBE-SST2, HadISST2, and HadSST3 products, in that they all tend to be cooler than buoy SSTs and warmer than independent CCI data. Comparatively, CMA-SST is closest to ERSST.v5, with similar analysis techniques, and its biases are lower than HadISST2 and HadSST3 at high latitudes of the Southern Hemisphere where in situ observations are limited. Second, comparison of their trends reveals similar year-to-year variations of CMA-SST to those of the congeneric products and a warming rate of CMA-SST within the range of the congeneric products over the period 2000–2019. In addition, CMA-SST expli-

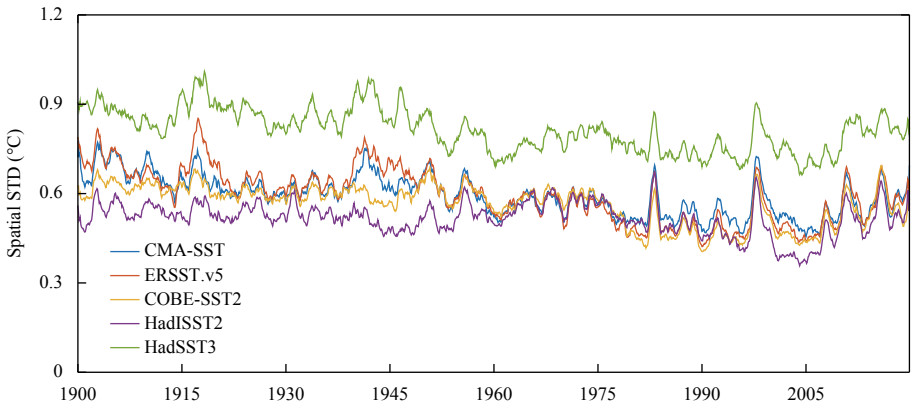

Fig. 10. Spatial STDs of monthly SSTAs from CMA-SST, ERSST.v5, COBE-SST2, HadISST2, and HadSST3 from 1900 to 2019. The SSTAs are set to be relative to their own climatologies over 1981–2010.

citly captures the two warming periods before the mid-1940s and after the mid-1970s, as well as the shut-down of the warming trend between them, and moreover an accelerating warming rate in most regions of the globe. Third, the Niño-3.4 and AMO index time series estimated by CMA-SST are nearly identical to those derived from the congeneric products, including the shape of the trend and the peak values and times. This indicates that CMA-SST is useful for investigating extreme marine climate events such as ENSO. Nonetheless, several differences between CMA-SST and the congeneric products are detected. For example, the warming rates of CMA-SST are slightly higher than those of the other products in many regions during 1900–2019 and 1950–2019, albeit the differences are within the quantified uncertainties of ERSST.v5. Moreover, the monthly differences in globally averaged SSTAs between CMA-SST and the congeneric products are assessed to be within the 95% confidence interval of the differences for all the datasets. The rationality of these differences in CMA-SST were also confirmed in a previous study, which pointed out that SST gridded analyses will never become identical, although they will continue to improve (Kent et al., 2017).

The assessments also indicate the need for further improvements involving in situ observations, bias correction, and reconstruction techniques for CMA-SST. First, compared with other regions, CMA-SST has substantially lower correlations with COBE-SST2, HadISST2, and HadSST3 at around 60°S, which might be due to the highly limited sampling of observations in this area, which necessitates the collection of more in situ observations, especially in data-sparse areas such as the Southern Ocean. Second, although an upgrade of a specific parameter for the SR02 bias correction technique has been investigated and shown its ability in locally improving the accuracy of the reconstructed SSTs, innovations are still needed to make the biases estimated by the SR02 method more realistic. For example, the assumption of constant SST–NMAT differences over time needs to be adjusted, to remove the biases stemming from trend differences in sea surface and atmospheric temperatures at local scales (Christy et al., 2001). Third, the differences in the strength and stability of the spatial STDs among the various datasets indicate the importance of proper reconstruction, especially in the data-sparse period. In future work, various SST reanalysis products in the satellite era besides OISST need to be compared and investigated, in order to optimize the applied base functions of EOTs. Besides, uncertainty estimations of CMA-SST are necessary in order to outline the varying degrees of impact of different parameters on reconstructed SSTs and provide guidance on parameter optimization, especially with respect to more accurate reconstruction where in situ observations are limited.

Acknowledgments. We thank Huang Boyin (NOAA/NCEI) for his valuable information on recent developments of key techniques applied in centennial SST analysis products, especially ERSST.v5.

REFERENCES

Cai, W. J., and T. Cowan, 2013: Why is the amplitude of the Indian Ocean Dipole overly large in CMIP3 and CMIP5 climate models? *Geophys. Res. Lett.*, **40**, 1200–1205, doi: 10.1002/grl.50208.

Chen, L. F., C. H. Sun, D. B. Zhang, et al., 2019: Bias correction and the dataset development of sea surface temperature over the Indian-Pacific Ocean from 1901 to 2016. *Chinese J. Geophys.*, **62**, 2001–2015, doi: 10.6038/cjg2019M0141. (in Chinese)

Christy, J. R., D. E. Parker, S. J. Brown, et al., 2001: Differential trends in tropical sea surface and atmospheric temperatures since 1979. *Geophys. Res. Lett.*, **28**, 183–186, doi: 10.1029/2000GL011167.

Freeman, E., S. D. Woodruff, S. J. Worley, et al., 2017: ICOADS Release 3.0: a major update to the historical marine climate record. *Int. J. Climatol.*, **37**, 2211–2232, doi: 10.1002/joc.4775.

Hirahara, S., M. Ishii, and Y. Fukuda, 2014: Centennial-scale sea surface temperature analysis and its uncertainty. *J. Climate*, **27**, 57–75, doi: 10.1175/JCLI-D-12-00837.1.

Huang, B. Y., V. F. Banzon, E. Freeman, et al., 2015: Extended Reconstructed Sea Surface Temperature version 4 (ERSST.v4). Part I: Upgrades and intercomparisons. *J. Climate*, **28**, 911–930, doi: 10.1175/JCLI-D-14-00006.1.

Huang, B. Y., P. W. Thorne, T. M. Smith, et al., 2016a: Further exploring and quantifying uncertainties for Extended Reconstructed Sea Surface Temperature (ERSST) version 4 (v4). *J. Climate*, **29**, 3119–3142, doi: 10.1175/JCLI-D-15-0430.1.

Huang, B. Y., M. L'Heureux, Z.-Z. Hu, et al., 2016b: Ranking the strongest ENSO events while incorporating SST uncertainty. *Geophys. Res. Lett.*, **43**, 9165–9172, doi: 10.1002/2016GL070888.

Huang, B. Y., P. W. Thorne, V. F. Banzon, et al., 2017: Extended Reconstructed Sea Surface Temperature, version 5 (ERSSTv5): Upgrades, validations, and intercomparisons. *J. Climate*, **30**, 8179–8205, doi: 10.1175/JCLI-D-16-0836.1.

Huang, B. Y., C. Y. Liu, G. Y. Ren, et al., 2019: The role of buoy and Argo observations in two SST analyses in the global and tropical Pacific Oceans. *J. Climate*, **32**, 2517–2535, doi: 10.1175/JCLI-D-18-0368.1.

Huang, Y. Y., and H. J. Wang, 2020: A possible approach for decadal prediction of the PDO. *J. Meteor. Res.*, **34**, 63–72, doi: 10.1007/s13351-020-9144-4.

IPCC, 2013: *Climate Change 2013*: *The Physical Science Basis*. *Contribution of Working Group I to the Fifth Assessment Report of the Intergovernmental Panel on Climate Change*, Stocker, T. F., D. Qin, G.-K. Plattner, et al., Eds., Cambridge University Press, Cambridge, United Kingdom and New

York, NY, USA, 1535 pp.

Ishii, M., A. Shouji, S. Sugimoto, et al., 2005: Objective analyses of sea-surface temperature and marine meteorological variables for the 20th century using ICOADS and the Kobe Collection. *Int. J. Climatol.*, **25**, 865–879, doi: 10.1002/joc.1169.

Karl, T. R., A. Arguez, B. Y. Huang, et al., 2015: Possible artifacts of data biases in the recent global surface warming hiatus. *Science*, **348**, 1469–1472, doi: 10.1126/science.aaa5632.

Kennedy, J. J., 2014: A review of uncertainty in in situ measurements and data sets of sea surface temperature. *Rev. Geophys.*, **52**, 1–32, doi: 10.1002/2013RG000434.

Kennedy, J. J., N. A. Rayner, C. P. Atkinson, et al., 2019: An ensemble data set of sea surface temperature change from 1850: The Met Office Hadley Centre HadSST.4.0.0.0 data set. *J. Geophys. Res. Atmos.*, **124**, 7719–7763, doi: 10.1029/2018JD029867.

Kent, E. C., N. A. Rayner, D. I. Berry, et al., 2013: Global analysis of night marine air temperature and its uncertainty since 1880: The HadNMAT2 data set. *J. Geophys. Res. Atmos.*, **118**, 1281–1298, doi: 10.1002/jgrd.50152.

Kent, E. C., J. J. Kennedy, T. M. Smith, et al., 2017: A call for new approaches to quantifying biases in observations of sea surface temperature. *Bull. Amer. Meteor. Soc.*, **98**, 1601–1616, doi: 10.1175/BAMS-D-15-00251.1.

Lau, N.-C., and M. J. Nath, 2004: Coupled GCM simulation of atmosphere–ocean variability associated with zonally asymmetric SST changes in the tropical Indian Ocean. *J. Climate*, **17**, 245–265, doi: 10.1175/1520-0442(2004)017<0245:CGSOAV>2.0.CO;2.

Liu, S. F., and A. M. Duan, 2017: Impacts of the leading modes of tropical Indian Ocean sea surface temperature anomaly on sub-seasonal evolution of the circulation and rainfall over East Asia during boreal spring and summer. *J. Meteor. Res.*, **31**, 171–186, doi: 10.1007/s13351-016-6093-z.

Merchant, C. J., O. Embury, J. Roberts-Jones, et al., 2014: Sea surface temperature datasets for climate applications from phase 1 of the European Space Agency Climate Change Initiative (SST CCI). *Geosci. Data J.*, **1**, 179–191, doi: 10.1002/gdj3.20.

Murphy, L. N., K. Bellomo, M. Cane, et al., 2017: The role of historical forcings in simulating the observed Atlantic multidecadal oscillation. *Geophys. Res. Lett.*, **44**, 2472–2480, doi: 10.1002/2016GL071337.

Rayner, N. A., D. E. Parker, E. B. Horton, et al., 2003: Global analyses of sea surface temperature, sea ice, and night marine air temperature since the late nineteenth century. *J. Geophys. Res. Atmos.*, **108**, 4407, doi: 10.1029/2002JD002670.

Ren, H.-L., R. Wang, P. M. Zhai, et al., 2017: Upper-ocean dynamical features and prediction of the super El Niño in 2015/16: A comparison with the cases in 1982/83 and 1997/98. *J. Meteor. Res.*, **31**, 278–294, doi: 10.1007/s13351-017-6194-3.

Reynolds, R. W., T. M. Smith, C. Y. Liu, et al., 2007: Daily high-resolution-blended analyses for sea surface temperature. *J. Climate*, **20**, 5473–5496, doi: 10.1175/2007JCLI1824.1.

Smith, T. M., and R. W. Reynolds, 1998: A high-resolution global sea surface temperature climatology for the 1961–90 base period. *J. Climate*, **11**, 3320–3323, doi: 10.1175/1520-0442(1998)011<3320:AHRGSS>2.0.CO;2.

Smith, T. M., and R. W. Reynolds, 2002: Bias corrections for historical sea surface temperatures based on marine air temperatures. *J. Climate*, **15**, 73–87, doi: 10.1175/1520-0442(2002)015<0073:BCFHSS>2.0.CO;2.

Smith, T. M., and R. W. Reynolds, 2003: Extended reconstruction of global sea surface temperatures based on COADS data (1854–1997). *J. Climate*, **16**, 1495–1510, doi: 10.1175/1520-0442(2003)016<1495:EROGSS>2.0.CO;2.

Titchner, H. A., and N. A. Rayner, 2014: The Met Office Hadley Centre sea ice and sea surface temperature data set, version 2: 1. Sea ice concentrations. *J. Geophys. Res. Atmos.*, **119**, 2864–2889, doi: 10.1002/2013JD020316.

Trenberth, K. E., 1997: The definition of El Niño. *Bull. Amer. Meteor. Soc.*, **78**, 2771–2778, doi: 10.1175/1520-0477(1997)078<2771:TDOENO>2.0.CO;2.

van den Dool, H. M., S. Saha, and Å. Johansson, 2000: Empirical orthogonal teleconnections. *J. Climate*, **13**, 1421–1435, doi: 10.1175/1520-0442(2000)013<1421:EOT>2.0.CO;2.

Yasunaka, S., and K. Hanawa, 2011: Intercomparison of historical sea surface temperature datasets. *Int. J. Climatol.*, **31**, 1056–1073, doi: 10.1002/joc.2104.

Zhang, Y., J. M. Wallace, and D. S. Battisti, 1997: ENSO-like interdecadal variability: 1900–93. *J. Climate*, **10**, 1004–1020, doi: 10.1175/1520-0442(1997)010<1004:ELIV>2.0.CO;2.

Zhou, X. B., Y. M. Tang, and Z. W. Deng, 2009: Assimilation of historical SST data for long-term ENSO retrospective forecasts. *Ocean Model.*, **30**, 143–154, doi: 10.1016/j.ocemod.2009.06.015.

Tech & Copy Editor: Qi WANG